AIAA JOURNAL
Vol. 36, No. 10, October 1998

Layerwise Theory for Dynamic Buckling and Postbuckling of Laminated Composite Cylindrical Shells

M. R. Eslami,* M. Shariyat,† and M. Shakeri‡
Amirkabir University of Technology, Tehran 15914, Iran

A general layerwise theory for dynamic buckling and postbuckling of imperfect multilayered composite circular cylindrical shells is introduced. In contrast to the conventional displacement-based layerwise theories that are more suitable for semianalytical solutions and kinematic boundary conditions, the present method includes the displacement and stress components at the same time. Thus, the method provides an efficient formulation where both kinematic and force boundary conditions can be exactly satisfied. To use the exact expressions of strain and stress components, the full Green's strain tensor for large deflections of circular cylinders is employed. Then almost no simplification is made in the development of the governing equations. The applied loads can be composed of various mechanical loads (axial compression, external pressure, external fluid pressure, and torsion or a combination of them). Accuracy and convergence of the present theory, in comparison with the three-dimensional elasticity approaches proposed so far, are higher and more effective. Finally, a few examples of various references that have used different theories are reexamined for comparison purpose.

Introduction

COMPOSITE structures in general have a low transverse shear modulus compared with the metallic ones. To achieve a higher strength, the composite components are chosen thicker. As a consequence, the transverse shear and transverse normal stresses play a more important role in the analysis of composite laminated structures than in metallic ones.

Investigations of the buckling phenomenon of circular cylindrical composite shells are concentrated on the static buckling of perfect shells. Recent investigations appear in Refs. 1–14.

The classical nonlinear shell theory suggested by Donnell,[15] which has formed the basis of many investigations in buckling analysis of shells, does not include the transverse shear and normal stresses and strains. However, Donnell's equilibrium and stability equations are used to predict the buckling behavior of composite laminated shells. For example, see Refs. 16–20. Results of the work of Kardomateas[12] reveal that neglecting these terms in the governing equations can lead to up to 120% error in prediction of the buckling loads.

In many references the effects of the transverse normal and shear stresses and strains are considered by means of higher-order strain-displacement expressions.[5,21–25] Recently, a high-order shear-deformation theory, which is very efficient in satisfying stress and displacement boundary conditions, was proposed by Eslami and Shariyat.[26]

In the works mentioned, the composite laminated shell is modeled by the equivalent single-layer theory.[27] According to this theory, the composite laminate is modeled by a single layer where the displacement components and their first derivatives across the thickness are approximated by continuous functions. Although these theories provide a sufficiently accurate description of the global laminate response, they are not capable of accurately determining interlaminar stresses near discontinuities such as holes, traction-free edges, and layer interfaces. For determining the three-dimensional stress field at the ply level, another class of theories, called layerwise theories, is provided. Improvement of these types of theories is mainly due to Robbins and Reddy[27] and Reddy and Savoia.[28] Although the proposed formulations can produce much more accurate results, they are displacement based and suffer from the point that moment, force, or stress boundary conditions (for example, simply supported edge conditions) cannot be incorporated accurately.

More recently, the authors of Refs. 9–13 have proposed some formulations to employ the three-dimensional elasticity theory for buckling analysis of orthotropic cylindrical shells. The proposed formulations are given for static buckling analysis of perfect single-layer-thick orthotropic shells. Eslami and Shariyat[29] have used the three-dimensional elasticity theory with the full nonlinear Green's strain tensor to study the buckling and postbuckling of perfect and imperfect orthotropic cylindrical shells. This study, which is restricted to single-layer cylindrical shells, includes the mechanical and thermal buckling analysis and discusses the full satisfaction of the kinematic as well as force boundary conditions.

The objective of the present paper is to develop a layerwise theory that possesses full three-dimensional modeling capability and satisfies both displacement and stress (or force and moment) boundary conditions. For this purpose, all of the strain and stress components are considered in the formulations and the exact expressions of strain-displacement components are derived by means of the full Green's strain tensor for large deflections of imperfect circular cylindrical shells. The dynamic loads are assumed to include mechanical loads such as axial compression, external pressure, external fluid pressure, and torsion or a combination of them. No simplification other than the Kantorovich type of solution is made. One of the major advantages of the proposed theory over the three-dimensional elasticity analysis (such as the accurate and general one proposed by Eslami and Shariyat[29]) is that the solution of full nonlinear governing equations of the present analysis shows more convergency. The resulting equations are solved using a fourth-order finite difference method with respect to spatial coordinates and a fourth-order Runge–Kutta method for time marching. An iterative scheme of solution is used in each time step to improve the results. Buckling loads are predicated based on Ref. 30 or increasing amplitude criteria. Finally, for comparison purposes, examples of some references that have employed various theories are reexamined to see the improvement offered by the present approach.

Formulation

Strain-Displacement and Stress-Strain Expressions

To determine the dynamic buckling loads, the dynamic response of a cylindrical shell under a time-varying load must be investigated. This approach requires that the behavior of the shell slightly beyond the buckling point (postbuckling) be studied, too. The Green's strain

Received March 7, 1997; revision received March 25, 1998; accepted for publication May 8, 1998. Copyright © 1998 by the American Institute of Aeronautics and Astronautics, Inc. All rights reserved.

*Professor, Mechanical Engineering Department, Hafez Avenue 424. Associate Fellow AIAA.
†Ph.D. Student, Mechanical Engineering Department, Hafez Avenue 424.
‡Associate Professor, Mechanical Engineering Department, Hafez Avenue 424.

tensor for large deformations in its general form in curvilinear coordinates can be written as[31]

$$E_{ij} = \tfrac{1}{2}\big(U_i|_j + U_j|_i + U_\alpha|_i U^\alpha|_j\big) \tag{1}$$

where the symbol | stands for covariant derivative. The tensorial and physical components of the strains and displacements can be related through the following expressions:

$$u_i = \sqrt{g^{ii}}U_i = \sqrt{g_{ii}}U^i, \qquad \epsilon_{ij} = \sqrt{g^{ii}}\sqrt{g^{jj}}E_{ij} \tag{2}$$

where g_{ij} and g^{ij} are the Euclidean metric and the associated metric tensors, respectively. Expansion of Eq. (1) leads to the strain-displacement relations of a perfect circular cylindrical shell. These equations, after rearrangement and employing Eq. (2), are

$$\begin{aligned}
\epsilon_{rr} &= w_{,r} + \tfrac{1}{2}\big[(w_{,r})^2 + (v_{,r})^2 + (u_{,r})^2\big]\\
\epsilon_{\theta\theta} &= (1/r)(v_{,\theta} + w) + (1/2r^2)\big[(v_{,\theta} + w)^2 + (w_{,\theta} - v)^2 + (u_{,\theta})^2\big]\\
\epsilon_{xx} &= u_{,x} + \tfrac{1}{2}\big[(w_{,x})^2 + (v_{,x})^2 + (u_{,x})^2\big]\\
\epsilon_{r\theta} &= (1/2r)[r v_{,r} + (w_{,\theta} - v)(w_{,r} + 1) + (v_{,\theta} + w)v_{,r} + u_{,r}u_{,\theta}]\\
\epsilon_{rx} &= \tfrac{1}{2}[w_{,x}(1 + w_{,r}) + u_{,r} + v_{,r}v_{,x} + u_{,r}u_{,x}]\\
\epsilon_{x\theta} &= \tfrac{1}{2}[v_{,x} + (1/r)u_{,\theta}] + (1/2r)[v_{,x}(v_{,\theta} + w) + u_{,\theta}u_{,x} + w_{,x}(w_{,\theta} - v)]
\end{aligned} \tag{3}$$

where u, v, and w are the displacement components in the axial, circumferential, and radial directions, respectively. For an imperfect shell, some initial strains exist due to the initial deformations of the shell. These imperfections are usually in the radial direction. (Considering the presence of initial axial and circumferential imperfections does not alter the generality of the present discussion.) If w_0 is the initial radial imperfection, then one may assume the initial strains as $\epsilon_{ij0} \equiv \epsilon_{ij0}(w_0)$. Expressions of these strains can be obtained from Eq. (3) by substituting u, $v = 0$ and $w = w_0$. Thus, strains due to loading are derived by subtracting the final strains from the initial strains:

$$\epsilon_{ij} = \tilde{\epsilon}_{ij} - \epsilon_{ij0} \tag{4}$$

where $\tilde{\epsilon}_{ij} \equiv \tilde{\epsilon}_{ij}(u, v, w + w_0)$ are the final strains. Therefore, referring to Eqs. (3) and (4), the strain-displacement relations for imperfect shells become

$$\begin{aligned}
\epsilon_{rr} &= w_{,r} + \tfrac{1}{2}\big[(w_{,r})^2 + 2w_{,r}w_{0,r} + (v_{,r})^2 + (u_{,r})^2\big]\\
\epsilon_{\theta\theta} &= (1/r)(v_{,\theta} + w) + (1/2r^2)\big\{(v_{,\theta} + w + w_0)^2 + [(w + w_0)_{,\theta} - v]^2\\
&\quad + (u_{,\theta})^2 - w_0^2 - (w_{0,\theta})^2\big\}\\
\epsilon_{xx} &= u_{,x} + \tfrac{1}{2}\big[(w_{,x})^2 + 2w_{,x}w_{0,x} + (v_{,x})^2 + (u_{,x})^2\big]\\
\epsilon_{r\theta} &= \tfrac{1}{2}v_{,r} + (1/2r)[(w_{,\theta} - v)(w_{,r} + 1) - v w_{0,r} + w_{,r}w_{0,\theta}\\
&\quad + w_{,\theta}w_{0,r} + (v_{,\theta} + w + w_0)\, v_{,r} + u_{,r}u_{,\theta}]\\
\epsilon_{rx} &= \tfrac{1}{2}[w_{,x}(1 + w_{,r}) + w_{0,x}w_{,r} + w_{0,r}w_{,x} + u_{,r} + v_{,r}v_{,x} + u_{,r}u_{,x}]\\
\epsilon_{x\theta} &= \tfrac{1}{2}[v_{,x} + (1/r)u_{,\theta}] + (1/2r)[v_{,x}(v_{,\theta} + w + w_0) + u_{,\theta}u_{,x}\\
&\quad + (w + w_0)_{,x}(w_{,\theta} - v) + w_{,x}w_{0,\theta}]
\end{aligned} \tag{5}$$

The stress-strain relation of an orthotropic body in the orthotropic axes can be expressed as

$$\{\sigma^*\} = [Q]\{\epsilon^*\} \tag{6}$$

where $\{\sigma^*\}$ and $\{\epsilon^*\}$ are the stress and strain components and $[Q]$ is the stiffness matrix, in the orthotropic axes,

$$[Q] = [S]^{-1} \tag{7}$$

and

$$[S] = \begin{pmatrix}
1/E_1 & -\nu_{21}/E_2 & -\nu_{31}/E_3 & 0 & 0 & 0\\
-\nu_{12}/E_1 & 1/E_2 & -\nu_{32}/E_3 & 0 & 0 & 0\\
-\nu_{13}/E_1 & -\nu_{23}/E_2 & 1/E_3 & 0 & 0 & 0\\
0 & 0 & 0 & 1/2G_{12} & 0 & 0\\
0 & 0 & 0 & 0 & 1/2G_{13} & 0\\
0 & 0 & 0 & 0 & 0 & 1/2G_{23}
\end{pmatrix} \tag{8}$$

The transformation of the stress and strain tensors from the orthotropic axes of the shell to the geometrical coordinates yields the relation between the stress and strain components in these coordinates as

$$\{\epsilon\} = [\bar{T}]\{\epsilon^*\}, \qquad \{\sigma\} = [\bar{T}]\{\sigma^*\} \tag{9}$$

or, regarding Eqs. (6–9),

$$\{\sigma\} = [\bar{Q}]\{\epsilon\} \tag{10}$$

where the transformed stiffness matrix in geometrical coordinates $[\bar{Q}]$ is

$$[\bar{Q}] = [\bar{T}][Q][\bar{T}]^{-1} \tag{11}$$

and where $[\bar{T}]$ is the transformation matrix that is defined as

$$[\bar{T}] = \begin{pmatrix}
1 & 0 & 0 & 0 & 0 & 0\\
0 & \cos^2\theta & \sin^2\theta & 0 & 0 & \sin 2\theta\\
0 & \sin^2\theta & \cos^2\theta & 0 & 0 & -\sin 2\theta\\
0 & 0 & 0 & \cos\theta & \sin\theta & 0\\
0 & 0 & 0 & -\sin\theta & \cos\theta & 0\\
0 & -0.5\sin 2\theta & 0.5\sin 2\theta & 0 & 0 & \cos 2\theta
\end{pmatrix} \tag{12}$$

Development of Hamilton's Functional

The equations of motion can be derived by using Hamilton's principle. Hamilton's principle for an elastic body in the absence of body forces is[32]

$$\int_{t_1}^{t_2}\left\{\int_S\int_{r_{\text{in}}}^{r_{\text{out}}}(\sigma_{ij}\delta\epsilon_{ij} + \rho\ddot{u}_i\delta u_i)\,\mathrm{d}r\cdot\mathrm{d}S - \delta\Omega\right\}\mathrm{d}t = 0 \tag{13}$$

where ρ is the density per unit volume and Ω is the work done by the external forces. According to Brush and Almroth,[33] for a circular cylindrical shell under external fluid pressure, this work is equal to

$$\Omega = p\int_{\bar{S}}\left[\bar{w} + \frac{1}{2\bar{r}}\big(\bar{v}^2 - \bar{v}\bar{w}_{,\theta} + \bar{v}_{,\theta}\bar{w} + \bar{w}^2\big)\right]\mathrm{d}\bar{S} \tag{14}$$

where $\bar{S}$ is the external surface of the shell and $\bar{v}$ and $\bar{w}$ are the circumferential and radial displacement components of this surface. For a shell under external pressure, only the first term in the preceding integral will appear.[33] The increments of the strain components can be readily found from Eq. (5). After some rearrangement, these expressions are

$$\begin{aligned}
\delta\epsilon_{rr} &= u_{,r}\delta u_{,r} + v_{,r}\delta v_{,r} + [1 + (w + w_0)_{,r}]\delta w_{,r}\\
\delta\epsilon_{\theta\theta} &= (1/r)\{-(1/r)[(w + w_0)_{,\theta} - v]\delta v + [1 + (1/r)(v_{,\theta} + w\\
&\quad + w_0)]\delta w + (1/r)u_{,\theta}\delta u_{,\theta} + [1 + (1/r)(v_{,\theta} + w + w_0)]\delta v_{,\theta}\\
&\quad + (1/r)[(w + w_0)_{,\theta} - v]\delta w_{,\theta}\}\\
\delta\epsilon_{xx} &= (1 + u_{,x})\delta u_{,x} + v_{,x}\delta v_{,x} + (w + w_0)_{,x}\delta w_{,x}
\end{aligned}$$

$$\delta\epsilon_{r\theta} = (1/2r)\{-[1+(w+w_0)_{,r}]\delta v + v_{,r}\delta w + u_{,\theta}\delta u_{,r} + (r+v_{,\theta}+w+w_0)\delta v_{,r} + [(w+w_0)_{,\theta} - v]\delta w_{,r} + u_{,r}\delta u_{,\theta} + v_{,r}\delta v_{,\theta} + [1+(w+w_0)_{,r}]\delta w_{,\theta}\}$$

$$\delta\epsilon_{rx} = \tfrac{1}{2}\{(1+u_{,x})\delta u_{,r} + v_{,x}\delta v_{,r} + (w+w_0)_x\delta w_{,r} + u_{,r}\delta u_{,x} + v_{,r}\delta v_{,x} + [1+(w+w_0)_{,r}]\delta w_{,x}\}$$

$$\delta\epsilon_{\theta,x} = (1/2r)\{-(w+w_0)_{,x}\delta v + v_{,x}\delta w + (1+u_{,x})\delta u_{,\theta} + v_{,x}\delta v_{,\theta} + (w+w_0)_{,x}\delta w_{,\theta} + u_{,\theta}\delta u_{,x} + [r+(v_{,\theta}+w+w_0)]\delta v_{,x} + [(w+w_0)_{,\theta} - v]\delta w_{,x}\} \tag{15}$$

Substituting Eq. (15) in Eq. (13) leads to

$$\int_{t_1}^{t_2}\left\{\int_S\left[\int_{r_{\text{in}}}^{r_{\text{out}}}\left(\rho\ddot{u}\delta u - \frac{1}{r}\left\{\frac{1}{r}\sigma_\theta[(w+w_0)_{,\theta} - v] + \sigma_{r\theta}[1+(w+w_0)_{,r}] + \sigma_{\theta x}(w+w_0)_{,x} - \rho r\ddot{v}\right\}\delta v + \frac{1}{r}\left\{\frac{1}{r}\sigma_\theta(r+v_{,\theta}+w+w_0) + \sigma_{r\theta}v_{,r} + \sigma_{\theta x}v_{,x} + \rho r\ddot{w}\right\}\delta w + \left\{\sigma_r u_{,r} + \frac{1}{r}\sigma_{r\theta}u_{,\theta} + \sigma_{rx}(1+u_{,x})\right\}\delta u_{,r} + \left\{\sigma_r v_{,r} + \frac{1}{r}\sigma_{r\theta}(r+v_{,\theta}+w+w_0) + \sigma_{rx}v_{,x}\right\}\delta v_{,r} + \left\{\sigma_r[1+(w+w_0)_{,r}] + \frac{1}{r}\sigma_{r\theta}[(w+w_0)_{,\theta} - v] + \sigma_{rx}(w+w_0)_{,x}\right\}\delta w_{,r} + \frac{1}{r}\left\{\frac{1}{r}\sigma_\theta u_{,\theta} + \sigma_{r\theta}u_{,r} + \sigma_{\theta x}(1+u_{,x})\right\}\delta u_{,\theta} + \frac{1}{r}\left\{\frac{1}{r}\sigma_\theta(r+v_{,\theta}+w+w_0) + \sigma_{r\theta}v_{,r} + \sigma_{\theta x}v_{,x}\right\}\delta v_{,\theta} + \frac{1}{r}\left\{\frac{1}{r}\sigma_\theta[(w+w_0)_{,\theta} - v] + \sigma_{r\theta}[1+(w+w_0)_{,r}] + \sigma_{\theta x}\times(w+w_0)_{,x}\right\}\delta w_{,\theta} + \left\{\sigma_x(1+u_{,x}) + \sigma_{rx}u_{,r} + \frac{1}{r}\sigma_{\theta x}u_{,\theta}\right\}\delta u_{,x} + \left\{\sigma_x v_{,x} + \sigma_{rx}v_{,r} + \frac{1}{r}\sigma_{\theta x}(r+v_{,\theta}+w+w_0)\right\}\delta v_{,x} + \left\{\sigma_x(w+w_0)_{,x} + \sigma_{rx}[1+(w+w_0)_{,r}] + \frac{1}{r}\sigma_{\theta x}[(w+w_0)_{,\theta} - v]\right\}\delta w_{,x}\right)\cdot \mathrm{d}r\right]\cdot \mathrm{d}S - \int_{\bar{S}}\frac{p}{2\bar{r}}\{(2\bar{v} - \bar{w}_{,\theta})\delta\bar{v} + [2\bar{r} + (\bar{v}_{,\theta} + 2\bar{w})]\delta\bar{w} + \bar{w}\delta\bar{v}_{,\theta} - \bar{v}\delta\bar{w}_{,\theta}\}\cdot \mathrm{d}\bar{S}\right\}\cdot \mathrm{d}t = 0 \tag{16}$$

In derivation of Hamilton's functional, as given by the preceding expression, the works of lateral forces are included explicitly. The works of the external loads applied to the ends of the shell are not explicitly considered. However, the effects of these end forces are considered when force boundary conditions are applied.

Integrating by parts in the x and θ directions leads to the following expression for Eq. (16):

$$\int_{t_1}^{t_2}\left\{\int_S\left[\int_{r_{\text{in}}}^{r_{\text{out}}}\left\{\rho\ddot{u} - \left[\left[\frac{1}{r}\sigma_\theta u_{,\theta} + \sigma_{r\theta}u_{,r} + \sigma_{\theta x}(1+u_{,x})\right]_{,\theta} + [r\sigma_x(1+u_{,x}) + r\sigma_{rx}u_{,r} + \sigma_{\theta x}u_{,\theta}]_{,x}\right]\right\}\delta u + [r\sigma_r u_{,r} + \sigma_{r\theta}u_{,\theta} + r\sigma_{rx}(1+u_{,x})]\delta u_{,r} - \left\{\left[\frac{1}{r}\sigma_\theta[(w+w_0)_{,\theta} - v] + \sigma_{r\theta}[1+(w+w_0)_{,r}] + \sigma_{\theta x}(w+w_0)_{,x} - \rho r\ddot{v}\right] + \left[\frac{1}{r}\sigma_\theta(r+v_{,\theta}+w+w_0) + \sigma_{r\theta}v_{,r} + \sigma_{\theta x}v_{,x}\right]_{,\theta} + [r\sigma_x v_{,x} + r\sigma_{rx}v_{,r} + \sigma_{\theta x}(r+v_{,\theta}+w+w_0)]_{,x}\right\}\delta v + [r\sigma_r v_{,r} + \sigma_{r\theta}(r+v_{,\theta}+w+w_0) + r\sigma_{rx}v_{,x}]\delta v_{,r} + \left\{\frac{1}{r}\sigma_\theta\times(r+v_{,\theta}+w+w_0) + \sigma_{r\theta}v_{,r} + \sigma_{\theta x}v_{,x} + \rho r\ddot{w} - \left[\frac{1}{r}\sigma_\theta\times[(w+w_0)_{,\theta} - v] + \sigma_{r\theta}[1+(w+w_0)_{,r}] + \sigma_{\theta x}(w+w_0)_{,x}\right]_{,\theta} - [r\sigma_x\times(w+w_0)_{,x} + r\sigma_{rx}[1+(w+w_0)_{,r}] + \sigma_{\theta x}[(w+w_0)_{,\theta} - v]]_{,x}\right\}\delta w + [r\sigma_r[1+(w+w_0)_{,r}] + \sigma_{r\theta}[(w+w_0)_{,\theta} - v] + r\sigma_{rx}(w+w_0)_{,x}]\times\delta w_{,r} - p(\bar{v} - \bar{w}_{,\theta})\delta\bar{v} + [\bar{r} + (\bar{v}_{,\theta} + \bar{w})]\delta\bar{w}\right]\mathrm{d}\theta\cdot\mathrm{d}x\right\}\cdot\mathrm{d}t = 0 \tag{17}$$

Layerwise Formulations

A Kantorovich type of approximation is used to derive the governing equations of the imperfect, multilayered composite shell. Accordingly, variations of the displacement components through the shell thickness are assumed independent of their variations in the x and θ directions. Furthermore, displacement variation trends within the kth layer are assumed to be different from those of the neighboring layers. Therefore, we can write

$$u_i^{(k)}(r,\theta,x,t) = \langle\phi(r)\rangle^{(k)}\{U_i(\theta,x,t)\} \qquad (k = 1,\ldots,N) \tag{18}$$

where $\langle\phi(r)\rangle^{(k)}$ is the shape function matrix of the kth layer and $\{U_i(\theta,x,t)\}$ is the displacement vector of grid points chosen through the thickness of the layer to enable approximation of the displacement components' variations in this direction. Then, if $(n+1)$ grid points are adopted, an alternative form of Eq. (18) is

$$u_i^{(k)} = \sum_{j=0}^{n^{(k)}}\left[U_i^{(k)}\right]_j\cdot\phi_j^{(k)}(r) \qquad (k = 1,\ldots,N) \tag{19}$$

Because $(n+1)$ points are selected in each layer, the approximation functions $\phi_j(r)$ are assumed to be polynomials of order n. A more suitable interpolation polynomial in the form of Eq. (19) is the Lagrange interpolating polynomial, in this situation,

$$\phi_j(r) = \prod_{\substack{i=0\\ i\neq j}}^{n}\frac{r - r_i}{r_j - r_i} \tag{20}$$

hence,

$$u_{i,r} = \sum_{j=0}^{n}\phi_{j,r}\cdot(U_i)_j = \sum_{j=0}^{n}\sum_{\substack{s=0\\ s\neq j}}^{n}\frac{1}{r_j - r_s}\prod_{\substack{i=0\\ i\neq j\\ i\neq s}}^{n}\frac{r - r_i}{r_j - r_i}(U_i)_j \tag{21}$$

and

$$\delta u_i^{(k)} = \sum_{j=0}^{n^{(k)}} \delta\left[U_i^{(k)}\right]_j \cdot \phi_j^{(k)}(r) \qquad (k = 1, \ldots, N) \tag{22}$$

where $\delta[U_i^{(k)}]_j$ are values of δu_i in the grid points. As may be noticed, each point of the shell has three degrees of freedom: $U_j^{(k)}$, $V_j^{(k)}$, and $W_j^{(k)}$. It is evident that these terms are repeated in the interpolating polynomials of the neighboring layers for grid points located at the common interface. Therefore, if Eq. (22) is substituted into Eq. (17), the terms are rearranged with respect to $\delta U_j^{(k)}$, $\delta V_j^{(k)}$, and $\delta W_j^{(k)}$, and it is noted that these values are arbitrary and nonzero, the resulted governing equations for internal points of each layer are

$$\int_{r_k}^{r_{k+1}} \Bigg(\Bigg\{ \Bigg[\frac{1}{r}\sigma_\theta u_{,\theta} + \sigma_{r\theta} u_{,r} + \sigma_{\theta x}(1+u_{,x}) \Bigg]_{,\theta} + [r\{\sigma_x(1+u_{,x}) + r\sigma_{rx}u_{,r} + \sigma_{\theta x}u_{,\theta}\}]_{,x} \Bigg] - \rho r\ddot{u} \Bigg\} \phi_j^{(k)} + \{r\sigma_r u_{,r} + \sigma_{r\theta}u_{,\theta} + r\sigma_{rx}(1+u_{,x})\}\phi_{j,r}^{(k)} \Bigg) \cdot \mathrm{d}r = 0$$

$$\int_{r_k}^{r_{k+1}} \Bigg(\Bigg\{ \frac{1}{r}\sigma_\theta[(w+w_0)_{,\theta} - v] + \sigma_{r\theta}[1+(w+w_0)_{,r}] + \sigma_{\theta x}(w+w_0)_{,x} - \rho r\ddot{v} \Bigg\} + \Bigg\{ \Bigg[\frac{1}{r}\sigma_\theta(r + v_{,\theta} + w + w_0) + \sigma_{r\theta}v_{,r} + \sigma_{\theta x}v_{,x} \Bigg]_{,\theta} + [r\sigma_x v_{,x} + r\sigma_{rx}v_{,r} + \sigma_{\theta x}(r + v_{,\theta} + w + w_0)]_{,x} \Bigg\} \phi_j^{(k)} - [r\sigma_r v_{,r} + \sigma_{r\theta}(r + v_{,\theta} + w + w_0) + r\sigma_{rx}v_{,x}]\phi_{j,r}^{(k)} \Bigg) \cdot \mathrm{d}r = 0 \tag{23}$$

$$\int_{r_k}^{r_{k+1}} \Bigg(\Bigg\{ \frac{1}{r}\sigma_\theta(r + v_{,\theta} + w + w_0) + \sigma_{r\theta}v_{,r} + \sigma_{\theta x}v_{,x} + \rho r\ddot{w} - \Bigg[\frac{1}{r}\sigma_\theta[(w+w_0)_{,\theta} - v] + \sigma_{r\theta}[1+(w+w_0)_{,r}] + \sigma_{\theta x}(w+w_0)_{,x} \Bigg]_{,\theta} - [r\sigma_x(w+w_0)_{,x} + r\sigma_{rx}[1+(w+w_0)_{,r}] + \sigma_{\theta x}[(w+w_0)_{,\theta} - v]]_{,x} \Bigg\} \phi_j^{(k)} + [r\sigma_r[1+(w+w_0)_{,r}] + \sigma_{r\theta}[(w+w_0)_{,\theta} - v] + r\sigma_{rx}(w+w_0)_{,x}]\phi_{j,r}^{(k)} \Bigg) \cdot \mathrm{d}r = 0$$

and for grid points located in the interfaces,

$$\int_{r_{k-1}}^{r_k} \Bigg(\Bigg\{ \Bigg[\frac{1}{r}\sigma_\theta u_{,\theta} + \sigma_{r\theta}u_{,r} + \sigma_{\theta x}(1+u_{,x}) \Bigg]_{,\theta} + [r\sigma_x(1+u_{,x}) + r\sigma_{rx}u_{,r} + \sigma_{\theta x}u_{,\theta}]_{,x} \Bigg] - \rho r\ddot{u} \Bigg\} \phi_{n^{(k-1)}}^{(k-1)} - \{r\sigma_r u_{,r} + \sigma_{r\theta}u_{,\theta} + r\sigma_{rx}(1+u_{,x})\}\phi_{n^{(k-1)},r}^{(k-1)} \Bigg) \cdot \mathrm{d}r + \int_{r_k}^{r_{k+1}} \Bigg(\Bigg\{ \Bigg[\frac{1}{r}\sigma_\theta u_{,\theta} + \sigma_{r\theta}u_{,r} + \sigma_{\theta x}(1+u_{,x}) \Bigg]_{,\theta} + [r\sigma_x(1+u_{,x}) + r\sigma_{rx}u_{,r} + \sigma_{\theta x}u_{,\theta}]_{,x} \Bigg] - \rho r\ddot{u} \Bigg\} \phi_0^{(k)} - \{r\sigma_r u_{,r} + \sigma_{r\theta}u_{,\theta} + r\sigma_{rx}(1+u_{,x})\}\phi_{0,r}^{(k)} \Bigg) \cdot \mathrm{d}r = 0$$

$$\int_{r_{k-1}}^{r_k} \Bigg(\Bigg\{ \frac{1}{r}\sigma_\theta[(w+w_0)_{,\theta} - v] + \sigma_{r\theta}[1+(w+w_0)_{,r}] + \sigma_{\theta x}(w+w_0)_{,x} - \rho r\ddot{v} \Bigg\} + \Bigg\{ \Bigg[\frac{1}{r}\sigma_\theta(r + v_{,\theta} + w + w_0) + \sigma_{r\theta}v_{,r} + \sigma_{\theta x}v_{,x} \Bigg]_{,\theta} + [r\sigma_x v_{,x} + r\sigma_{rx}v_{,r} + \sigma_{\theta x}(r + v_{,\theta} + w + w_0)]_{,x} \Bigg\} \phi_{n^{(k-1)}}^{(k-1)} - [r\sigma_r v_{,r} + \sigma_{r\theta}(r + v_{,\theta} + w + w_0) + r\sigma_{rx}v_{,x}]\phi_{n^{(k-1)},r}^{(k-1)} \Bigg) \cdot \mathrm{d}r + \int_{r_k}^{r_{k+1}} \Bigg(\Bigg\{ \frac{1}{r}\sigma_\theta[(w+w_0)_{,\theta} - v] + \sigma_{r\theta}[1+(w+w_0)_{,r}] + \sigma_{\theta x}(w+w_0)_{,x} - \rho r\ddot{v} \Bigg\} + \Bigg\{ \Bigg[\frac{1}{r}\sigma_\theta(r + v_{,\theta} + w + w_0) + \sigma_{r\theta}v_{,r} + \sigma_{\theta x}v_{,x} \Bigg]_{,\theta} + [r\sigma_x v_{,x} + r\sigma_{rx}v_{,r} + \sigma_{\theta x}(r + v_{,\theta} + w + w_0)]_{,x} \Bigg\} \phi_0^{(k)} - [r\sigma_r v_{,r} + \sigma_{r\theta}(r + v_{,\theta} + w + w_0) + r\sigma_{rx}v_{,x}]\phi_{0,r}^{(k)} \Bigg) \cdot \mathrm{d}r = 0 \tag{24}$$

$$\int_{r_{k-1}}^{r_k} \Bigg(\Bigg\{ \frac{1}{r}\sigma_\theta(r + v_{,\theta} + w + w_0) + \sigma_{r\theta}v_{,r} + \sigma_{\theta x}v_{,x} + \rho r\ddot{w} - \Bigg[\frac{1}{r}\sigma_\theta \times [(w+w_0)_{,\theta} - v] + \sigma_{r\theta}[1+(w+w_0)_{,r}] + \sigma_{\theta x}(w+w_0)_{,x} \Bigg]_{,\theta} - [r\sigma_x(w+w_0)_{,x} + r\sigma_{rx}[1+(w+w_0)_{,r}] + \sigma_{\theta x}[(w+w_0)_{,\theta} - v]]_{,x} \Bigg\} \phi_{n^{(k-1)}}^{(k-1)} + [r\sigma_r[1+(w+w_0)_{,r}] + \sigma_{r\theta}[(w+w_0)_{,\theta} - v] + r\sigma_{rx}(w+w_0)_{,x}]\phi_{n^{(k-1)},r}^{(k-1)} \Bigg) \cdot \mathrm{d}r + \int_{r_k}^{r_{k+1}} \Bigg(\Bigg\{ \frac{1}{r}\sigma_\theta(r + v_{,\theta} + w + w_0) + \sigma_{r\theta}v_{,r} + \sigma_{\theta x}v_{,x} + \rho r\ddot{w} - \Bigg[\frac{1}{r}\sigma_\theta[(w+w_0)_{,\theta} - v] + \sigma_{r\theta}[1+(w+w_0)_{,r}] + \sigma_{\theta x}(w+w_0)_{,x} \Bigg]_{,\theta} - [r\sigma_x(w+w_0)_{,x} + r\sigma_{rx}[1+(w+w_0)_{,r}] + \sigma_{\theta x}[(w+w_0)_{,\theta} - v]]_{,x} \Bigg\} \phi_0^{(k)} + [r\sigma_r[1+(w+w_0)_{,r}] + \sigma_{r\theta}[(w+w_0)_{,\theta} - v] + r\sigma_{rx}(w+w_0)_{,x}]\phi_{0,r}^{(k)} \Bigg) \cdot \mathrm{d}r = 0$$

For grid points lying on the external surface of the shell, the expression $[+p(v^N - w_{,\theta}^N)\phi_j^N(r_{\text{out}})]$ must be added to the second equation of Eq. (23), and the expression $\{-p[r_{\text{out}} + (v_{,\theta}^N + w^N)]\phi_j^N(r_{\text{out}})\}$ must be added to the third one. Expressions having the superscript N correspond to points located on the outer surface of the shell.

Numerical Solution and Buckling Criteria

The governing equations (23) and (24) include multiplications of the stress terms in the displacement expressions. Thus, recalling that the stresses are nonlinear functions of the displacements, the resulting equations are coupled and are highly nonlinear functions of the displacements. Nonlinear problems of mechanics are often solved by adopting an incremental formulation. By the incremental solution procedure, the real time-variant system is assumed to have time invariance within each time step.

Rearrangement of Eqs. (23) and (24) leads to equations of the following type ($s = 1, 2, 3$; $j = 0, \ldots, m$) for each layer or interface:

$$f^m[\sigma_{ij}, U_i, w_0, U_{i,x}, w_{0,x}, U_{i,\theta}, w_{0,\theta}, (\ddot{U}_s)_j|_{j\neq m}] = I^k_{mm}(\ddot{U}_s)_m \qquad m = 0, \ldots, n^{(k-1)} \tag{25}$$

$$g\big[\sigma_{ij}, U_i, w_0, U_{i,x}, w_{0,x}, U_{i,\theta}, w_{0,\theta}, (\ddot{U}_s)^{(k)}_j\big|_{j\neq 0}, (\ddot{U}_s)^{(k-1)}_j\big|_{j\neq n^{(k-1)}}\big] = \big[I^k_{00} + I^{k-1}_{n^{(k-1)}n^{(k-1)}}\big](\ddot{U}_s)^{(k)}_0$$

$$h\big[\sigma_{ij}, U_i, w_0, U_{i,x}, w_{0,x}, U_{i,\theta}, w_{0,\theta}, (\ddot{U}_s)^{(N)}_j\big|_{j\neq N}\big] = I^N_{n^N n^N}\big(\ddot{U}^N_s\big)_N$$

where for $s = 2, 3$,

$$I^k_{mn} = \int_{r_k}^{r_{k+1}} r\cdot\rho\cdot\phi^{(k)}_m(r)\cdot\phi^{(k)}_n(r)\cdot \mathrm{d}r \tag{26}$$

and where for $s = 1$, the first term of the integrand, i.e., r, does not appear. The terms U_1, U_2, and U_3 are equivalent to U, V, and W, respectively. Therefore, the following expressions hold for the displacements in the time interval Δt[20,34]:

$$f^m[\tilde{\sigma}_{ij}, \tilde{U}_i, w_0, \tilde{U}_{i,x}, w_{0,x}, \tilde{U}_{i,\theta}, w_{0,\theta}, (\ddot{U}_s)_j|_{j\neq m}] = I^k_{mm}(\Delta\ddot{U}_s)_m \qquad m = 0, \ldots, n^{(k-1)}$$

$$g\big[\tilde{\sigma}_{ij}, \tilde{U}_i, w_0, \tilde{U}_{i,x}, w_{0,x}, \tilde{U}_{i,\theta}, w_{0,\theta}, (\ddot{U}_s)^{(k)}_j\big|_{j\neq 0}, (\ddot{U}_s)^{(k-1)}_j\big|_{j\neq n^{(k-1)}}\big] = \big[I^k_{00} + I^{k-1}_{n^{(k-1)}n^{(k-1)}}\big](\Delta\ddot{U}_s)^{(k)}_0 \tag{27}$$

$$h\big[\tilde{\sigma}_{ij}, \tilde{U}_i, w_0, \tilde{U}_{i,x}, w_{0,x}, \tilde{U}_{i,\theta}, w_{0,\theta}, (\ddot{U}_s)^{(N)}_j\big|_{j\neq N}\big] = I^N_{n^N n^N}\big(\Delta\ddot{U}^N_s\big)_N$$

in which values corresponding to the end of the time interval are demonstrated by a tilde. Therefore

$$3\left\{\sum_{k=1}^{N}\big[n^{(k)}+1\big]\right\}$$

coupled and nonlinear equations in terms of ΔU_i, ΔV_i, and ΔW_i are obtained. The displacements should satisfy the following initial conditions, for $x = 0, L$ and $\theta = 0, 2\pi$:

$$\begin{aligned} &\Delta U_i = 0, && \Delta V_i = 0, && \Delta W_i = 0 \\ &\Delta\dot{U}_i = \dot{U}_i, && \Delta\dot{V}_i = \dot{V}_i, && \Delta\dot{W}_i = \dot{W}_i \end{aligned} \tag{28}$$

The numerical solution procedure is accomplished through the following steps:

1) The numerical solution begins with discretizing each of the internal and external surfaces as well as the interfaces into $m \times n$ grid points in the axial and circumferential directions, respectively. If more precision is required, each layer can be divided into many virtual layers with the same mechanical properties.

2) The initial geometric deviations of the shell at the grid points are defined, and the initial values of the displacement terms U_i are set to zero.

3) Corresponding increments of mechanical loads are found.

4) Starting from points lying near the fixed edges, derivative terms of U_i with respect to the spatial coordinates that appear in Eqs. (5), (23), and (24) are approximated by a second-order finite difference method (the central difference method).

5) Based on the displacement values (U_i, w_0) and their derivatives obtained in the grid points of each layer, the strain values are computed from Eq. (5). The displacement components are determined from Eq. (19), and their derivatives are computed from a similar equation.

6) The constitutive equations are considered, and using Eqs. (6–12), the stress components are calculated. It is evident that this step is not necessary for the boundary points if the stress boundary conditions are prescribed.

7) Derivatives in Eq. (27) involving multiplication of the stress components in the displacement terms (or their derivatives) are substituted using a fourth-order finite difference approximation.

8) In the process of solution, time invariance for terms that appeared in the first sides of Eq. (27) is assumed during each time step. Thus, values of $\ddot{U}_i$ of the left-hand side of the lower equations are substituted from the results of the higher equations of the current system of equations, and the remaining terms are replaced by the values obtained in the previous iterative step of the current time interval. Thus, a set of second-order differential equations is derived that can be solved using the fourth-order Runge–Kutta method subject to initial conditions that appeared in Eq. (28).

9) When all equations in each iterative step of the current time interval are solved, the maximum value of a displacement component (for example, the lateral displacement $w_{\max}$) is determined.

10) In each grid point, increments of the displacement components (ΔU_i) are added to displacement components obtained at the end of the previous time interval. To improve the results, the solution is continued by using more iterations starting from step 4, until the difference of the successive values of $w_{\max}$ of the same time interval becomes negligible.

11) The corrected values of U_i, $\dot{U}_i$ obtained in this manner are considered as initial values for the next time interval.

12) Beginning from step 3, results corresponding to the next time step are obtained.

13) The possibility of dynamic buckling occurrence is checked. For this purpose, variations of $w_{\max}$ vs time or vs applied load (external pressure, axial load, temperature gradient, etc.) are plotted. Buckling load can be determined using one of the two equivalent stability criteria stated next.

a) The generalized concept of dynamic buckling proposed by Budiansky[30] is associated with dynamic buckling of a structure where small changes in the magnitude of loading lead to large changes in the structure response. According to this criterion, abrupt reduction in slope of the maximum lateral displacement vs load curve (minimum slope) indicates a dynamic buckling state. The behavior of the structure beyond this point is called postbuckling.

b) Qualitively, if the time histories of the maximum lateral deformation or other modes of deformation are given for several amplitudes of the applied load, the critical buckling load can simply be defined as the load at which a large increase in the displacement amplitude of the deformations is seen to occur with time.[16]

These two criteria have a common mathematical basis and lead to identical results.[16] Postbuckling behavior can be investigated by studying the mentioned curves beyond the buckling point. (For this purpose, the Budiansky criterion is preferred.)

14) In the case of no buckling point, the amplitudes of the applied loads are increased, and calculations are continued starting from step 2.

Calculations and Results

Almost all examples of the well-known references in the field of dynamic buckling of composite multilayered cylindrical shells are restricted to studying buckling under mechanical loads. Thus, because the aims of the following examples are comparison among results of the various theories proposed so far and verification of the results obtained using the developed formulations, the adopted examples are consistent with buckling under mechanical loads. Besides, to avoid the occurrence of local extrema of the displacement field within each layer, second-order Lagrange interpolating polynomials $\phi^{(k)}_j$ are adopted.

Static Buckling Analysis Results

To compare the results of the present theory with those of the higher shear deformation equivalent layer theories, perfect cylinders of Ref. 5 having the following geometric and material properties are considered:

$$R = 19.05\,\text{cm}, \qquad R/h = 15$$

$$E_{11} = 206.844\times10^9\,\text{Pa}, \qquad E_{22} = 18.6159\times10^9\,\text{Pa}$$

$$E_{33} = 18.6159\times10^9\,\text{Pa}, \qquad G_{12} = 4.48162\times10^9\,\text{Pa}$$

$$G_{13} = 4.48162\times10^9\,\text{Pa}, \qquad G_{23} = 2.55107\times10^9\,\text{Pa}$$

$$\nu_{11} = 0.21, \qquad \nu_{13} = 0.21, \qquad \nu_{23} = 0.45$$

Table 1 Stacking sequences used

Code number	Stacking sequence
1	$[0_3]_s$
2	$[0/90/0]_s$
3	$[90/0/90]_s$
4	$[90_3]_s$
5	$[45_2/-45]_s$
6	$[45/-45_2]_s$
7	$[-45/45/-45]_s$
8	$[-45_2/45]_s$
9	$[30_2/-60]_s$

Table 2 Critical axial compression, (N/m) × 10^{-6}, for complete fixation of the ends

Code number	CL	FOSD	HOSDEL	GLW
$L/R=1$				
1	82.66	53.76	34.50	32.38
2	66.64	35.46	32.40	31.26
3	32.83	23.41	21.40	21.13
4	14.71	13.82	13.22	13.04
5	28.41	18.92	17.33	16.92
6	33.76	21.61	19.45	18.86
7	36.56	23.42	21.23	20.74
8	28.41	18.92	17.33	16.92
9	57.63	28.44	24.30	22.31
$L/R=5$				
1	12.52	12.71	12.45	12.37
2	15.77	14.98	14.76	14.52
3	15.11	14.01	13.72	13.48
4	11.38	10.67	10.54	10.49
5	14.50	12.76	12.41	12.35
6	17.45	14.93	14.38	14.32
7	20.66	17.06	16.12	15.86
8	14.50	12.76	12.41	12.35
9	12.03	10.66	10.12	9.89

Table 3 Critical pressure, Pa × 10^{-3}

Code number	CL	FOSD	HOSDEL	GLW
$L/R=1$				
1	1,847	1,771	1,765	1,758
2	6,687	6,274	6,191	6,126
3	15,671	14,286	14,196	14,147
4	20,512	18,567	18,333	18,218
5	6,226	5,805	5,743	5,689
6	6,226	5,839	5,791	5,714
7	6,226	5,853	5,826	5,804
8	6,226	5,805	5,743	5,689
9	3,144	2,999	2,985	2,974

Their stacking sequences are presented in Table 1. In Ref. 5, static buckling of perfect circular cylindrical shells using an equivalent layer approach is investigated by means of a displacement-based formulation. Two load cases are considered: a uniform axial compression with $L/R=1$, 5 and a lateral pressure on a very long cylinder. Critical loads corresponding to classical theory (CL), the first-order shear deformation theory (FOSD), the higher-order shear deformation and equivalent layer theory (HOSDEL) of Ref. 5, and the present generalized layerwise theory (GLW) are presented for axial compression (Table 2) and external pressure (Table 3). As noticed from Table 2, classical theory results overestimate the buckling loads especially for the shorter lengths. Table 3 reveals that for long cylinders results of the mentioned theories become closer and the difference becomes higher for thicker cylinders.

Another comparison is made with a conventional displacement-based layerwise theory proposed by Reddy and Savoia.[28] For this purpose, postbuckling of two imperfect three-layered, cross-ply (0/90/0) cylindrical shells, like those presented in Ref. 28, is investigated for different initial imperfections. The imperfection is assumed to have the form

$$w_0 = \sum_{m=1}^{M}\sum_{n=0}^{N} W_0^{mn}\sin\left(\frac{m\pi x}{L}\right)\cos(n\theta) \tag{29}$$

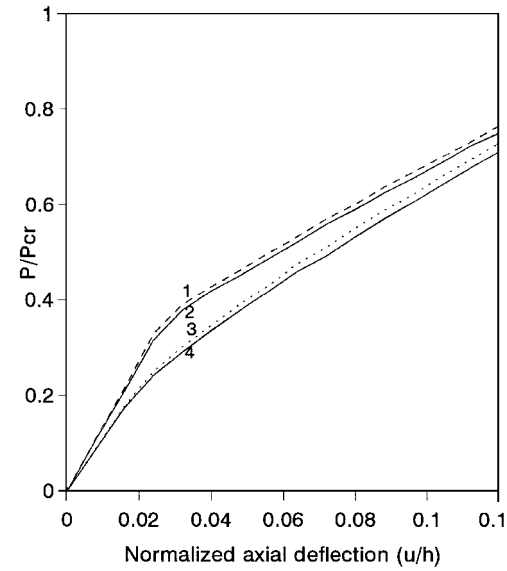

Fig. 1 Comparison of the postbuckling analysis results of a thin shell. The illustrated results correspond to the internal surface at $x=1$: ·¹·, $W^{mn}=-0.001$, Ref. 27; ——², $W^{mn}=-0.001$, present study; -·-³, $W^{mn}=-0.01$, Ref. 27; and——⁴, $W^{mn}=-0.01$, present study.

where m and n are the numbers of axial half-waves and circumferential waves, respectively.

The mechanical properties of the shell are

$$E_l = 209.5\,\text{GPa}, \qquad E_t = 7\,\text{GPa}$$

$$G_{lt} = 3.5\,\text{GPa}, \qquad G_{tt} = 1.4\,\text{GPa}$$

$$\nu_{lt} = \nu_{tt} = 0.3, \qquad h_i = h/3$$

where subscripts l and t stand for directions along and transverse to fibers, respectively. Two three-layered thin ($h=0.254$ cm) and moderately thick ($h=2.54$ cm) shells with $R=91.4$ cm and $l=254$ cm are considered.

Figure 1 shows the axial load vs the axial deflection curve of the thin shell for two different amplitudes of initial geometrical imperfections. Results of Ref. 28 and results of the present analysis are plotted simultaneously for comparison. As mentioned before, dynamic buckling occurs in points where an abrupt change in displacement modes (for example, axial deflection) due to a small increase in the applied loads is noticed. In Fig. 1, the axial load is normalized with respect to the static buckling load of the shell. The deformed shape and buckling modes of the cylindrical shell are shown in Fig. 2. The major disadvantage of the analysis presented in Ref. 28 is that the boundary conditions are not completely satisfied. Because of the incorporation of exact strain-displacement expressions in the present analysis, the present results are lower than the other results. At the end portion of the buckling curve of Fig. 2, based on the present analysis, the slope increases gradually. This is in agreement with the results reported in Refs. 20 and 34.

The postbuckling response for the moderately thick shell is presented in Fig. 3, and the deformed shape of the shell is illustrated in Fig. 4. A comparison of Figs. 2 and 4 reveals that, in thick cylindrical shells, in contrast to the thin shells, lower buckling modes are dominant. That is, in the limit, the thick cylindrical shells buckle in an axisymmetric manner.[15] The difference between the predicted critical loads of these theories increases for the moderately thick shell.

Finally, a comparison with the latest three-dimensional analysis proposed by Ref. 13 is done. The proposed formulations of the aforementioned reference are suitable for static buckling of thick perfect single-layer circular cylindrical shells under mechanical loads and are based on infinitesimal strain assumptions (linear strain-displacement expressions). In this paper the boundary conditions are satisfied in average, and the results are obtained using a finite difference method.

Table 4 gives a comparison of the predicted loads for a very long shell under external pressure. The critical pressures are normalized

Table 4 Comparison of the results of various theories for cylindrical shells under external pressure

Geometry	FOSD	HOSDEL[40]	P3D	GLW
Circumferential reinforcement				
$h = 6.35$ mm, $h/R = 0.03$, $L/R = 100$	0.9668	0.9637	0.9694	0.9608
$h = 12.7$ mm, $h/R = 0.07$, $L/R = 100$	0.9050	0.8933	0.9148	0.8892
Axial reinforcement				
$h = 6.35$ mm, $h/R = 0.03$, $L/R = 100$	0.9822	0.9822	0.9817	0.9816
$h = 12.7$ mm, $h/R = 0.07$, $L/R = 100$	0.9588	0.9556	0.9605	0.9528

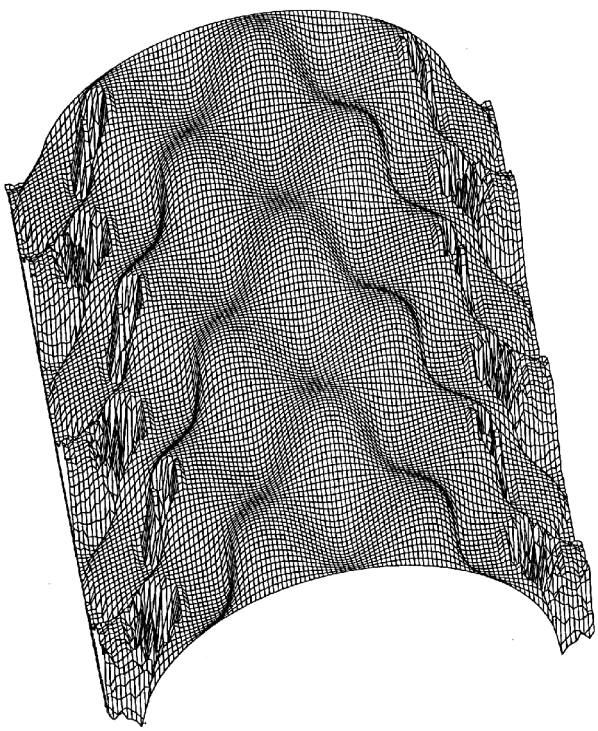

Fig. 2 Buckling mode of the thin cylindrical shell.

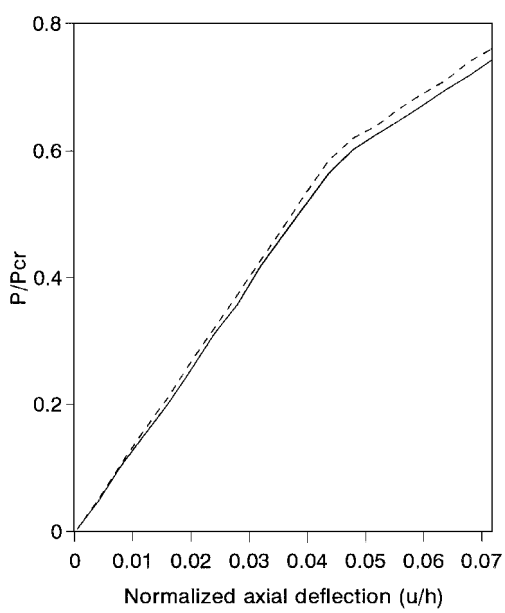

Fig. 3 Comparison of the postbuckling analysis results of a moderately thick shell. The illustrated results correspond to the internal surface at $x = 1$: - -, Ref. 27 ($W^{mn} = -0.001$), and ——, present paper.

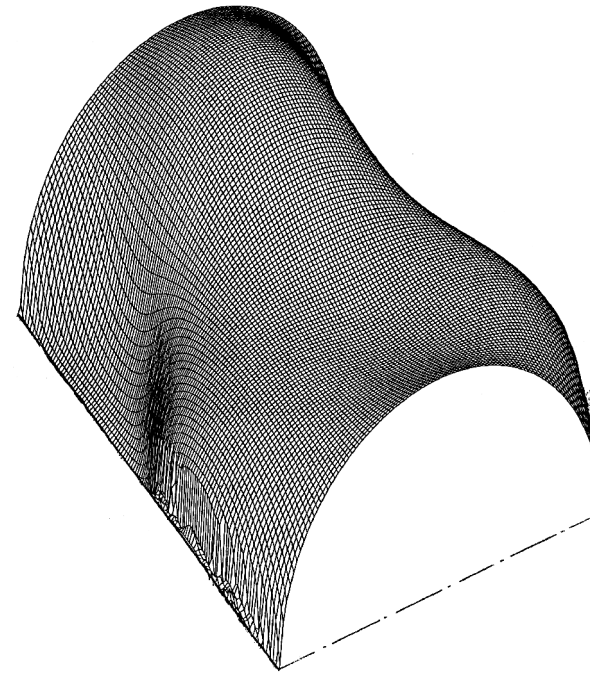

Fig. 4 Buckling mode of the thick cylindrical shell.

with respect to the classical theory (Donnell's shell theory) results. Two cases of material properties are considered: circumferential reinforcement ($E_2 \gg E_1, E_3$) and axial reinforcement ($E_3 \gg E_1, E_2$). Results of the preliminary three-dimensional analysis are denoted by P3D.

Dynamic Buckling

As a first example, the buckling of a four-ply laminated imperfect cylindrical shell under uniform axial compression of Refs. 35 and 17 is reexamined. The cylinder is considered to be simply supported with radius $R = 19.0$ cm and $L/R = 2$. The thickness of each layer is 0.0135 cm, and the laminate construction is [0/30/60/90]. The material of each lamina is boron/epoxy, AVCO 550, with the following properties:

$$E_x = 207\,\text{GPa}, \qquad E_\theta = 18.6\,\text{GPa}, \qquad G_{x\theta} = 4.48\,\text{GPa}$$

$$\nu_{x\theta} = \nu_{xz} = \nu_{z\theta} = 0.21$$

The initial geometric imperfections of the shell are defined as

$$w_0(x, \theta) = W_0 h \cdot \sin(\pi_x / L) \cdot \cos(8\theta) \tag{30}$$

where W_0 is the amplitude coefficient of imperfection and h is the total thickness of the shell.

The results of the dynamic buckling analysis performed by Refs. 17 and 35, as well as the present results, are depicted in Fig. 5. In the earlier results, an equivalent layer approach is adopted and von-Kármán-type expressions of strains are chosen. The results of Ref. 35 are based on the Hoff–Simitses criterion (the total potential energy approach), which is explained in detail in Ref. 36, so that the static and dynamic loads for $W_0 = 0$ are identical. In Ref. 17, Love–Kirchhoff assumptions are employed, and the nonlinear equations of motion are linearized and solved using an incremental method described in Ref. 16. As seen from Fig. 5, the reduction in buckling loads is diminished as the imperfection amplitude increases. In other words, imperfection sensitivity is more noticeable in small imperfection amplitudes. In comparison with the other results, the present formulation gives smaller critical loads. This is due to incorporation of the exact strain-displacement relations in the governing equations. The results are compatible with the exact three-dimensional elasticity analysis.

Figure 6 shows the effect of various impulsive loads (rectangular, triangular, and parabolic impulsive loads) and their time duration on

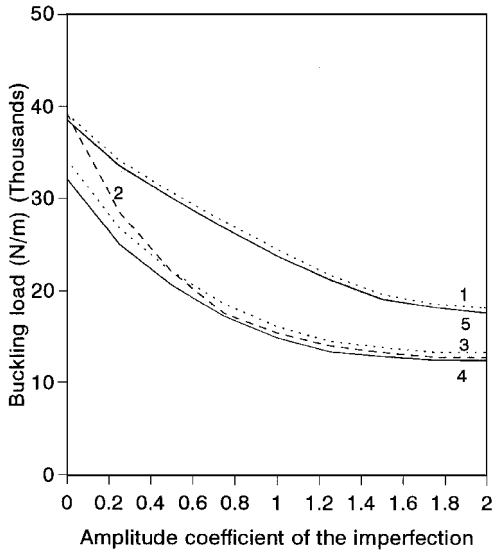

Fig. 5 Effect of imperfection amplitude on the dynamic buckling load: ·¹·, Sheinman, Liaw (static); ²-, Sheinman et al. (dynamic); ·³·, Liaw and Yang (dynamic); ⁴——, present study (dynamic); and ⁵——, present study (static).

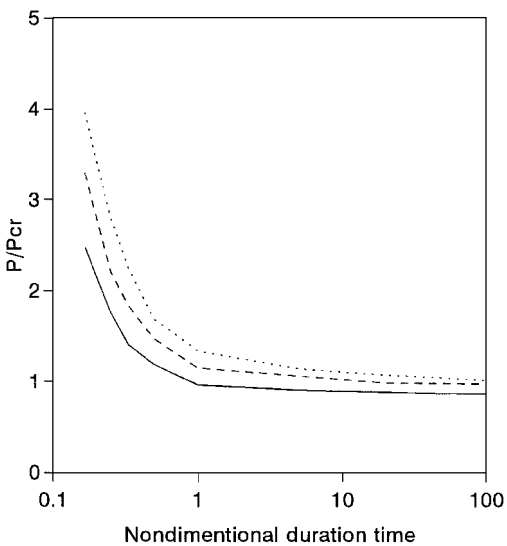

Fig. 6 Effect of different types of impulsive loads and various loading durations on the buckling load of the cylindrical shell: ——, rectangular impulse; - - - -, parabolic impulse; and ···--, triangular impulse.

the predicted critical loads. For this purpose, the following nondimensional time is used:

$$t^* = \bar{\tau}/\bar{\tau}_0 \tag{31}$$

where $\bar{\tau}$ is the pulse duration and $\bar{\tau}_0$ is the free vibration period of the shell. In Fig. 6, P_{cr} is the static buckling load. These results indicate that shell stiffness increases for a short duration of loading (especially if the pulse duration is comparable to the hoop breathing mode). For short time durations, the dynamic buckling loads are larger than the static buckling load. It is believed that this phenomenon is due to the stress wave revibration between the impacted and fixed ends of the shell.[37–39] For a given amplitude, the step load has a maximum curve area. Thus, as may be expected, this type of loading has the worst influence on the strength of the shell. The critical loads corresponding to the triangular impulsive loads are the largest.

The second example of the static analysis is reconsidered, and the dynamic buckling due to dynamic axial load is investigated. The results of the analysis are shown in Fig. 7. The reduction in the dynamic buckling load for the thick shell is more than that of the thin shell. The reason is that the effects of transverse shear and normal stresses are more significant in thick shells.

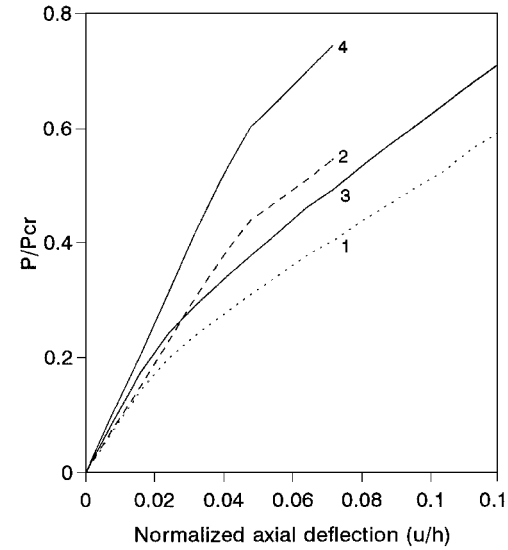

Fig. 7 Comparison between the dynamic and the static buckling results of the thin and thick shells. The illustrated results correspond to the internal surface at $x = 1$ and $W^{mn} = -0.01$: ·¹·, thin shell, dynamic; ²-, thick shell, dynamic; ³——, thin shell, static; and ⁴——, thick shell, static.

Conclusion

Based on the exact kinematic relations of the three-dimensional theory of elasticity, a general layerwise theory is introduced. The proposed formulations may be employed for dynamic buckling analysis of cylindrical shells with various boundary conditions. Although run time and instability of the present results are higher than in the conventional equivalent layer theories, they pose the accuracy of the exact three-dimensional theory of elasticity with higher convergency.

From the illustrated results, the following conclusions may be deduced:

1) In comparison to the axial compression loading, results of various theories show less difference in the case of external pressure loading.

2) External loadings that are applied in the form of a step function result in minimum buckling loads.

3) Loads with time duration less than the free vibration period lead to dynamic buckling loads that are higher than the static ones.

4) The dynamic-to-static-buckling-load ratio is smaller for thicker shells.

5) Buckling loads predicted by the equivalent layer theories overestimate the actual buckling loads.

6) Imperfection sensitivity is more noticeable in small initial geometric deviations.

7) Lower buckling modes are more magnified in thicker shells.

8) Fixing the total thickness of the shell, stability increases with increasing number of layers.

9) The influence of the transverse shear and normal stress is more remarkable for smaller orthotropy ratios (G_{ij}/E_1, E_i/E_1) and thicker shells.

10) The discrepancy among various theories is greater for antisymmetric stacking sequences and decreases with increasing shell length.

References

[1] Thangaratnam, R. K., Palaninathan, R., and Ramachandran, J., "Thermal Buckling of Laminated Composite Shells," *AIAA Journal*, Vol. 28, No. 5, 1990, pp. 859, 860.

[2] Ma, S. F., and Wilcox, M. W., "Thermal Buckling of Axisymmetric Angle-Ply Laminated Cylindrical Shells," *Composite Engineering*, Vol. 1, No. 3, 1991, pp. 183–192.

[3] Huang, N. N., and Tauchert, T. R., "Large Deflection of Laminated Cylindrical and Doubly Curved Panels Under Thermal Loading," *Computer and Structure Journal*, Vol. 41, No. 2, 1991, pp. 303–312.

[4] Kossira, H., and Haupt, M., "Buckling of Laminated Plates and Cylindrical Shells Subjected to Combined Thermal and Mechanical Loads," *Buckling of Shell Structures, on Land, in the Sea and in the Air*, edited by J. F. Jullien, Elsevier, New York, 1991, pp. 201–212.

[5]Simitses, G. J., and Anastasiadis, J. S., "Shear Deformable Theories for Cylindrical Laminates—Equilibrium and Buckling with Applications," *AIAA Journal*, Vol. 30, No. 3, 1992, pp. 826–834.

[6]Shen, H. S., and Williams, F. W., "Postbuckling Analysis of Stiffened Laminated Panels Loaded in Compression," *International Journal of Solids and Structures*, Vol. 30, No. 12, 1993, pp. 1589–1630.

[7]Weller, T., and Patlashenko, I., "Postbuckling of Infinite Length Cylindrical Panels Under Combined Thermal and Pressure Loading," *International Journal of Solids and Structures*, Vol. 30, No. 12, 1993, pp. 1649–1662.

[8]Song, Y., Sheinman, I., and Simitses, G. J., "Thermoelastoviscoplastic Buckling Behavior of Cylindrical Shells," *Journal of Engineering Mechanics*, Vol. 121, No. 1, 1995, pp. 62–70.

[9]Kardomateas, G. A., "Buckling of Thick Orthotropic Cylindrical Shells Under External Pressure," *Journal of Applied Mechanics*, Vol. 60, March 1993, pp. 195–202.

[10]Kardomateas, G. A., "Stability Loss in Thick Transversely Isotropic Cylindrical Shells Under Axial Compression," *Journal of Applied Mechanics*, Vol. 60, June 1993, pp. 506–513.

[11]Kardomateas, G. A., and Chung, C. B., "Buckling of Thick Orthotropic Cylindrical Shells Under External Pressure Based on Non-Planar Equilibrium Modes," *International Journal of Solids and Structures*, Vol. 31, No. 16, 1994, pp. 2195–2210.

[12]Kardomateas, G. A., "Bifurcation of Equilibrium in Thick Orthotropic Cylindrical Shells Under Axial Compression," *Journal of Applied Mechanics*, Vol. 62, March 1995, pp. 43–52.

[13]Kardomateas, G. A., and Philobos, M. S., "Buckling of Thick Orthotropic Cylindrical Shells Under Combined External Pressure and Axial Compression," *AIAA Journal*, Vol. 33, No. 10, 1995, pp. 1946–1953.

[14]Eslami, M. R., and Shariyat, M., "Elastic-Plastic and Creep Buckling of Imperfect Cylinders Under Mechanical and Thermal Loading," *Journal of Pressure Vessel Technology*, Vol. 119, Feb. 1997, pp. 27–36.

[15]Donnell, L. H., *Beams, Plates, and Shells*, McGraw–Hill, New York, 1976, Chap. 4.

[16]Saigal, S., Yang, T. Y., and Kapania, R. K., "Dynamic Buckling of Imperfection-Sensitive Shell Structures," *AIAA Journal*, Vol. 24, No. 10, 1987, pp. 718–724.

[17]Liaw, D. G., and Yang, T. Y., "Symmetric and Asymmetric Dynamic Buckling of Laminated Thin Shells," *Journal of Composite Materials*, Vol. 24, Feb. 1990, pp. 188–207.

[18]Argento, A., and Scott, R. A., "Dynamic Instability of Layered Anisotropic Circular Cylindrical Shells, Part I: Theoretical Development," *Journal of Sound and Vibration*, Vol. 162, No. 2, 1993, pp. 311–322.

[19]Kasagi, A., and Sridharan, S., "Imperfection Sensitivity Layered Composite Cylinders," *Journal of Engineering Mechanics*, Vol. 121, No. 7, 1995, pp. 810–818.

[20]Shariyat, M., and Eslami, M. R., "A Hybrid Higher-Order Theory for Thermal Dynamic Buckling Analysis of Imperfect Laminated Cylindrical Shells," *Computer and Structure Journal* (submitted for publication).

[21]Zukas, J. A., "Effect of Transverse Normal and Shear Strains in Orthotropic Shells," *AIAA Journal*, Vol. 12, No. 12, 1974, pp. 1753–1755.

[22]Reddy, J. N., and Liu, C. F., "A Higher-Order Shear Deformation Theory of Laminated Elastic Shells," *International Journal of Engineering Science*, Vol. 23, No. 3, 1985, pp. 319–330.

[23]Stein, M., "Nonlinear Theory for Plates and Shells Including the Effect of Transverse Bending," *AIAA Journal*, Vol. 24, No. 9, 1986, pp. 1537–1544.

[24]Dennis, S. T., and Palazotto, A. N., "Transverse Shear Deformation in Orthotropic Cylindrical Pressure Vessels Using a Higher-Order Shear Theory," *AIAA Journal*, Vol. 27, No. 10, 1989, pp. 1441–1447.

[25]Barbero, E. J., Reddy, J. N., and Teply, J. L., "General Two-Dimensional Theory of Laminated Cylindrical Shells," *AIAA Journal*, Vol. 28, No. 3, 1990, pp. 544–553.

[26]Eslami, M. R., and Shariyat, M., "Dynamic Buckling and Postbuckling of Imperfect Laminated Cylindrical Shells Under Mechanical and Thermal Loads, Using a High Order Shear-Deformation Theory," *Journal of Pressure Vessel Technology* (submitted for publication).

[27]Robbins, J. R., and Reddy, J. N., "Modelling of Thick Composites Using a Layerwise Laminate Theory," *International Journal of Numerical Methods Engineering*, Vol. 36, No. 4, 1993, pp. 655–677.

[28]Reddy, J. N., and Savoia, M., "Layer-Wise Shell Theory for Postbuckling of Laminated Circular Cylindrical Shells," *AIAA Journal*, Vol. 30, No. 8, 1992, pp. 2148–2154.

[29]Eslami, M. R., and Shariyat, M., "Dynamic Buckling and Postbuckling of Imperfect Orthotropic Cylindrical Shells Under Mechanical and Thermal Loads, Based on the Three Dimensional Theory of Elasticity," *Journal of Applied Mechanics* (submitted for publication).

[30]Budiansky, B., "Theory of Buckling and Postbuckling Behavior of Elastic Structures," *Advances in Applied Mechanics*, No. 1, 1974, pp. 1–65.

[31]Flugge, W., *Tensor Analysis and Continuum Mechanics*, Pergamon, New York, 1972, p. 28.

[32]Washizu, K., *Variational Methods in Elasticity and Plasticity*, Pergamon, UK, 1982, p. 152.

[33]Brush, D. O., and Almroth, B. O., *Buckling of Bars, Plates and Shells*, McGraw–Hill, New York, 1975, p. 160.

[34]Gillat, R., Feldman, E., and Aboudi, J., "Axisymmetric Response of Nonlinearly Elastic Cylindrical Shells to Dynamic Axial Load," *International Journal of Impact Engineering*, Vol. 13, No. 4, 1993, pp. 545–554.

[35]Shienman, I., Shaw, I. D., and Simitses, G. J., "Nonlinear Analysis of Axially Loaded Laminated Cylindrical Shells," *Computer and Structure Journal*, Vol. 16, 1983, pp. 131–137.

[36]Simitses, G. J., *Dynamic Stability of Suddenly Loaded Structures*, Springer–Verlag, Berlin, 1990, p. 6.

[37]Lindberg, H. E., "Dynamic Buckling of Cylindrical Shells from Oscillating Waves Following Axial Impact," *International Journal of Solids and Structures*, Pt. 1, Vol. 23, No. 6, 1987, pp. 669–692.

[38]Lindberg, H. E., "Dynamic Pulse Buckling of Imperfection Sensitive Shells," *Journal of Applied Mechanics*, Vol. 58, Sept. 1991, pp. 743–748.

[39]Zimcik, D. G., and Tennyson, R. C., "Stability of Circular Cylindrical Shells Under Transient Axial Impulsive Loading," *AIAA Journal*, Vol. 18, No. 6, 1980, pp. 691–699.

G. A. Kardomateas
Associate Editor